Mon. Not. R. astr. Soc. (1989) **240,** 1009–1023

Hot gas in a cosmological *N*-body simulation

Peter Thomas[1]★ and R. G. Carlberg[2]

[1] *Canadian Institute for Theoretical Astrophysics, 60, St George St, Toronto, Ontario, M5S 1A1, Canada*

[2] *Department of Astronomy, University of Toronto, 60, St George St, Toronto, Ontario, M5S 1A1, Canada*

Accepted 1989 April 11. Received 1989 March 30; in original form 1988 November 11

Summary. We examine the properties of the hot gas in a cosmological *N*-body simulation. The cooling algorithm for the gas is discussed in some detail – it provides a quick and effective way of identifying the masses and positions of galaxies. Possible changes to the algorithm are discussed; however, these are unlikely to significantly improve the results. Two large clusters are visible at the final stage of our simulations. One of these is smooth and centrally condensed – reminiscent of nearby cooling flow clusters; the other is dynamically young, with an extended low-density core. Sunyaev–Zel'dovich fluctuations of microwave background photons in their passage through the hot gas are discussed. We conclude that the effect is small, $\langle \Delta T/T \rangle \lesssim 10^{-5}$, unless a cluster of galaxies is visible along the line-of-sight.

1 Introduction

Most of the estimated total baryonic density in the Universe, $\Omega_b \simeq 0.1$ (Yang *et al.* 1984; Audouze 1987), is inferred to be in the form of ionized gas (Gunn & Peterson 1965). The most readily detectable component outside of galaxies is the gas which finds its way into the dark haloes of galaxies and clusters where it is shock-heated to X-ray emitting temperatures (review by Sarazin 1986). This hot gas can Compton scatter microwave background photons to produce a small change in their measured temperature (Zel'dovich & Sunyaev 1969). These effects are valuable probes of the large-scale distribution of matter in the Universe, providing information that is independent of the galaxy distribution.

A previous paper (Carlberg & Couchman 1988, hereafter CC88) discussed the results of an *N*-body model that contained a gas component. It analysed the clustering and dynamics of the galaxies that formed from cooling gas in the simulation, finding a relatively small spatial bias in the clustering but a significant velocity bias of the galaxies with respect to the dark-matter background. In the simulations only about one-third of all the baryons ever formed into stars, and of all the stars only 10–20 per cent of them are in galaxies sufficiently luminous to be comparable to standard galaxies. Most of the baryons that remain as gas are heated to the virial equilibrium temperatures of the dark-matter haloes that they inhabit.

★Present address: Astronomy Centre, Division of Physics and Astronomy, University of Sussex, Falmer, Brighton BN1 9QH.

In this paper we examine the properties of the hot gas in the CC88 simulations, make a quantitative estimate of the perturbations to the MWB and discuss the X-ray emission characteristics of two characteristic clusters of galaxies in the simulation.

2 The numerical model

2.1 OVERVIEW

The numerical model used in Carlberg (1988a,b) and CC88 is designed to break the clustering hierarchy of the collisionless dark matter by creating dissipated stellar galaxies. The simulations use 64^3 gas and 64^3 dark particles of mass $1.5\times10^9 M_\odot$ and $1.5\times10^{10} M_\odot$ each, respectively, within a $[40/(1+z)\,\mathrm{Mpc}]^3$ periodic box ($\Omega=1$, $H_0=50$ km s^{-1} Mpc^{-1}). The gravitational forces are evaluated for both components using a particle–particle particle–mesh (PPPM) method on a 64^3 grid with a softening length of 13 kpc. The CDM spectrum is normalized to give a bias parameter of 1.5 at the final time – although the final state might be slightly under-evolved; see CC88 for more details.

Star formation is controlled by demanding that the gas has a cooling time shorter than a dynamical time of a galactic size mass. A simple set of two-body collision rules regulates the entire process, yielding a relatively inexpensive N-body code that has been demonstrated to create appropriate numbers of galaxies which have clearly separated away from the clustering hierarchy of the dark matter. A reasonable match can be made to the observed galaxy distribution.

2.2 PARTICLE INTERACTIONS

The gas physics in the simulations is based on a simple kinetic theory for particle interactions, but modified to allow for cooling and star formation. Below $\sim 10^6$ K the cooling function, Λ, is relatively large and increases to low temperatures; the cooling time is therefore short and gas will quickly cool to 10^4 K, below which Λ drops precipitously due to the recombination of hydrogen. At temperatures above $\sim 10^6$ K the cooling function is small and decreases to low

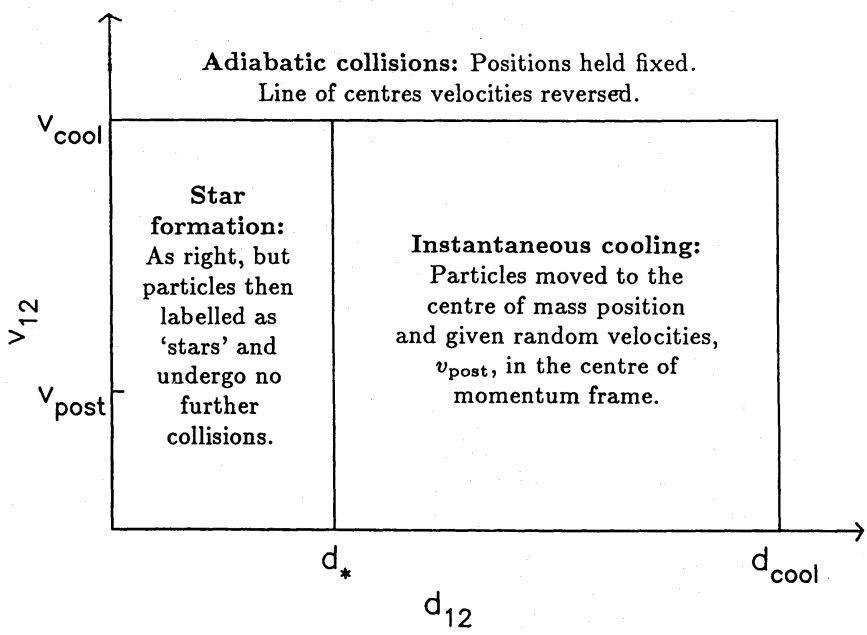

Figure 1. A summary of the outcome of two-body collisions in our simulations.

temperatures, resulting in a correspondingly long cooling time which is taken to be infinite (i.e. much longer than a Hubble time).

The cooling algorithm, based on two-body collisions, is outlined in Fig. 1. On every other time-step (for reasons of economy) particles are collided with the nearest approaching neighbour [within a $(625\ \mathrm{kpc}/1+z)^3$ box]. The result of the collision depends upon the relative separation, $d_{12}=|\mathbf{r}_1-\mathbf{r}_2|$, and the relative velocity along the line of centres $v_{12}=(\mathbf{v}_2-\mathbf{v}_1)\cdot(\mathbf{r}_1-\mathbf{r}_2)/d_{12}$:

(i) If $d_{12}>d_{\mathrm{cool}}$ or $v_{12}>v_{\mathrm{cool}}$ then an adiabatic collision takes place – each particle's position is held fixed but its velocity along the line of centres is reversed. d_{cool} corresponds to a density of $\sim 7\times10^{-4}\ \mathrm{cm}^{-3}$ and v_{12} to a temperature of 2.5×10^5 K. This represents the situation in which low-density or high-temperature gas does not cool appreciably in one time-step.

(ii) If $d_*<d_{12}<d_{\mathrm{cool}}$ and $v_{12}<v_{\mathrm{cool}}$ then the cooling time is considered sufficiently short that the gas will cool on less than a dynamical time. The particles are moved to the centre of mass position and given Gaussian random velocities of magnitude v_{post} in the centre of momentum frame. The actual rate of cooling does not matter, provided that it occurs before dynamical evolution disrupts the system; in practice the time-scale determined by the simulation time-step satisfies this condition.

(iii) If $d_{12}<d_*$ and $v_{12}<v_{\mathrm{cool}}$ (i.e. at sufficiently high densities) then the gas is formed into stellar material. The collision is handled as in (ii) but the particles are subsequently labelled as 'stars' and undergo no further collisions.

2.3 DENSITY

The cooling algorithm described above uses the nearest (approaching) neighbour distance to estimate the local density, although for a Poisson distribution of particles the expected mean density diverges logarithmically at small separations! In practice this divergence is limited by the finite resolution of the code and the removal of particles to form stars but there is nevertheless a wide range of measured densities. These fluctuations are unimportant, as it is the temperature rather than the density condition which determines the sites of cooling. Nevertheless, it would be easy to modify the algorithm to use the distance to the third or fourth nearest neighbour when calculating the density. The probability that the N'th nearest neighbour lies in the volume element $V\mapsto V+\delta V$ is given by

$$\delta P=P_{N-1}(V)\,\delta V=\frac{(\bar{n}V)^{N-1}}{(N-1)!}\exp(-\bar{n}V)\,\delta(\bar{n}V), \tag{1}$$

where $\bar{n}$ is the mean density and $P_{N-1}(V)$ is the probability that there are exactly $N-1$ neighbours within a volume V. Then the mean measured density (N/V) is $\bar{n}N/(N-1)$, with variance $[\bar{n}N/(N-1)]^2/(N-2)$ and the third nearest neighbour gives a reasonable estimate with a finite dispersion. Note that this procedure would not increase the integration time since these distances are evaluated when finding the nearest neighbour for collision.

2.4 TEMPERATURE

The two-particle temperature estimator $(\mu m_{\mathrm{H}}/3k)\sigma^2$, where $\sigma^2=\frac{3}{2}v_{12}^2$, is better behaved than that for the density. It averages to the correct value with variance $\mathrm{var}(\sigma^2)=2\sigma^4$. However, the line-of-sight velocity differences uses only a third of the information available on the relative velocity dispersion is $\Sigma_{i=1}^{N}(\mathbf{v}_i^2-\bar{\mathbf{v}}^2)/3(N-1)$. This has variance $2\sigma^4/3(N-1)$ and so, even for $N=2$, gives a lower dispersion than before. One possible hybrid scheme would be to use three

or more particles to estimate the local density and temperature and then to collide with the nearest approaching neighbour as outlined in Section 2.2 (it is necessary to collide with approaching particles only, so that cooled particles will not recollide on the following time-step). For reasons described in Section 2.6 below, we do not think this would significantly alter or improve our results.

2.5 TRANSPORT PROCESSES

One of the drawbacks of using kinetic theory with a limited number of particles is that transport processes can be important, especially in low-density regions. The transport coefficients for diffusion and viscosity are normally governed by particle interpenetration; the effect of collisions at a distance (particles are forced to collide with the nearest approaching neighbour within a 625-kpc box in order to prevent free streaming of gas flows through one another) is to limit these two effects but to increase the rate of heat conduction. Shock waves travel at the rate of one particle separation per collision time-step – which can exceed the speed of sound in low-density regions. A typical distance for diffusion is given by the total distance travelled by a particle divided by the square root of the number of collisions, which is approximately 0.5 Mpc over the lifetime of the experiment, independent of the local density.

2.6 HIGH-DENSITY GAS AND STAR FORMATION

The distribution of high-density gas is regulated by the details of the cooling and star-formation algorithm. The densities corresponding to separations, d_*, are unrealistically high and star formation only occurs when two pairs of particles are brought together by cooling. Thus the actual value of d_* makes little physical sense – it merely acts as a parameter to regulate the rate of conversion of cooling gas into stars. Fortunately, this seems to be a reasonable procedure as the results are not strongly dependent upon the particular value of d_* chosen; we merely require that star formation takes place sufficiently rapidly in regions where the cooling time is shorter than the dynamical time.

A detailed description of star formation would not be possible without models for reheating, metal injection etc. Nevertheless, our algorithm is designed to reproduce the galaxy formation scheme of White & Rees (1978) (see also Rees & Ostriker 1977; Silk 1977) as shown in Fig. 2.

Consider the ratio, τ, of the cooling time of primordial gas clouds (after turnaround and collapse) to their dynamical time (approximately equal to the Hubble time). Clouds with short cooling times ($\tau < 1$) can dissipate to form stellar material and galaxies, while those with long cooling times ($\tau > 1$) are disrupted by subsequent dynamical evolution and do not form bound objects. The region to the right of the solid line in this diagram is the range of parameter space in which galaxy formation can take place (for a metallicity of 0.4 solar as is observed for a wide range of clusters, Mushotzky 1984; Rothenflug & Arnaud 1985; Ulmer *et al.* 1987). The dashed lines show the various positions in this plane for virialized clouds of a given mass, depending upon their initial overdensity. As can be seen there is a cut-off at $\sim 10^{12} M_{\odot}$, relatively independent of overdensity, above which galaxies do not form; this limit is reduced if the gas has a lower metallicity. Larger galaxies form via mergers.

The relatively large variance of the temperature estimator used in our simulations means that the boundary between cooling and non-cooling regions in the density–temperature plane is not sharp. The dotted lines in Fig. 2 show the fraction of gas that can cool at a given mean density and temperature. Some cooling still occurs at higher temperatures although vigorous star formation takes place only when a large fraction of the particles can cool, below about 5×10^5 K; in some sense this is more realistic than the abrupt cut-off which would be obtained

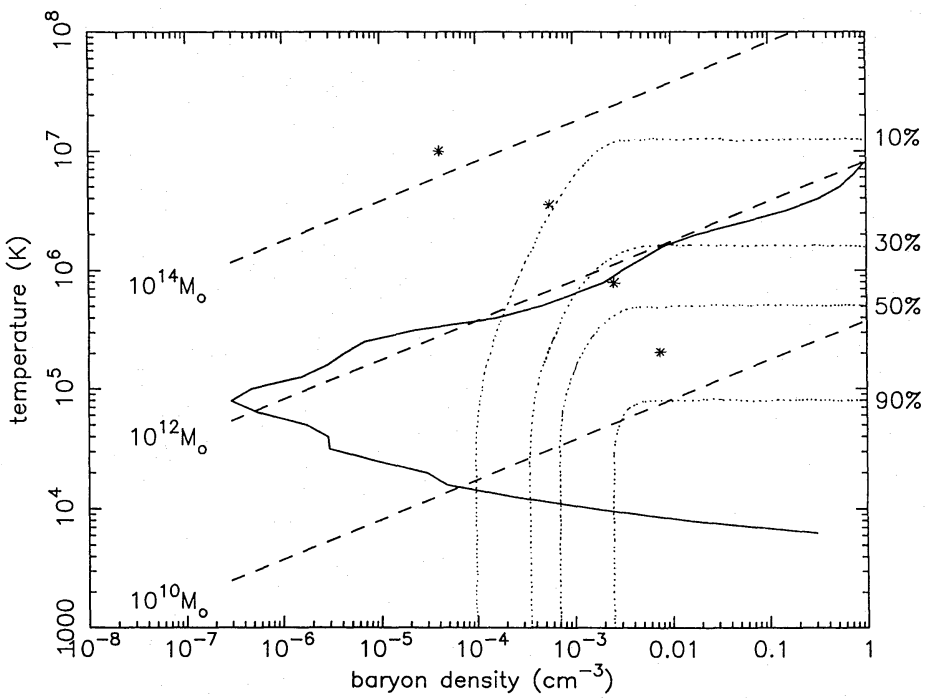

Figure 2. A summary of the fate of cooling, solar-metallicity gas clouds in the simple White & Rees (1978) model of galaxy formation. Clouds which lie to the right of the solid line have $\tau < 1$ and can dissipate to form galaxies, while those to the left are disrupted by hierarchical clustering. The dashed lines are loci of constant virialized mass. Haloes with overdensities of 100 lie around the positions shown by the *'s, at redshifts (from bottom right to top left) of 4.6, 2.8, 1.6 and 0. The dotted lines show what fraction of the gas particles in our simulation will cool at given density and temperature.

if the temperature were to be accurately determined, as the cooling function does not drop suddenly to zero at one temperature. The *'s mark the position of haloes with overdensities of 100; at early times ($z \gtrsim 3$) it is the temperature constraint which limits cooling, while at later times the density constraint takes over. Star formation is widespread at first, then becomes negligible as the virial temperature of collapsed structures increases. In practice the temperature constraint may be slightly too low, with star formation ceasing rather too early. There is little biasing of stellar material on large scales. Galaxies are identified by connecting stellar particles which lie within a given 'linking length' of one another – this amounts to specifying a particular overdensity. For this reason the galaxies are slightly biased, although not as severely as in many other models – see CC88 for more details.

3 Results of the simulations

3.1 MEASUREMENT PROCEDURE

In this section we examine the distribution of gas in the simulations, which involves looking at the structure on a wide range of scales. One way to do this would be to use the nearest neighbours algorithm as described in Section 2.2. However, as has been shown, this procedure is dominated by Poisson noise. Instead we divide the simulated volume into cells, each containing just a few particles, as follows: The whole volume is first partitioned into eight sub-cubes, and each of these into eight smaller sub-cubes ..., until a cube is reached with less than four particles in it. The union of this cube with those of its seven siblings which also contain less than four particles then defines a box whose contents are taken to be representative of this volume. Groups of less than four particles are not resolved by this procedure but as these

represent less than 4 per cent of the total number of particles we exclude these cells from the following analysis to improve the statistics of density and temperature measurements.

3.2 DENSITY

Fig. 3 shows the density distribution of particles in the 40 Mpc box at $z=0$. There are $64^3=262\,144$ gas particles and an equal number of CDM particles, each representing $1.5\times10^9 M_\odot$ or $1.5\times10^{10}M_\odot$, respectively. The mean baryon density, $\bar{n}_b$, corresponds to $\Omega_b=\frac{1}{11}$; an overdensity of 10^5 represents 5×10^{-2} cm^{-3}, which is similar to the observed density in the cores of clusters of galaxies. Approximately one third of the gas has condensed to form stars at this stage. One half of the remainder, with overdensities greater than a few, has settled into clusters; the number of gas particles at a given density follows a power law $dN/d\log n\propto n^{-1/2}$, which is of the form we expect if most of the gas is locked up in haloes with density profiles $n\propto r^{-2}$ since then we have $N(>n)\propto nr^3\propto n^{-1/2}$. Much of the residual gas is presumably falling into the outskirts of these clusters with less than one-fifth of the original gas remaining in underdense regions at the present.

At earlier times our simulations do not give a clear picture of the gas distribution within collapsed haloes. In those objects where the cooling time is shorter than the Hubble time our algorithm cools gas within a few time-steps, whereas the true cooling time may be longer. Thus, although the gas does cool in the correct place, it may do so more rapidly and so give lower densities than is really the case. The evolution of the lowest-density gas, associated with voids, is well represented by a simple model of spherical underdensities in an otherwise homogeneous Universe.

3.3 TEMPERATURE

Fig. 4 shows the 'phase diagram' of the gas (and dark matter) at $z=0$. Note that the dispersion in the temperature is real and vastly exceeds the estimator variance. When interpreting the

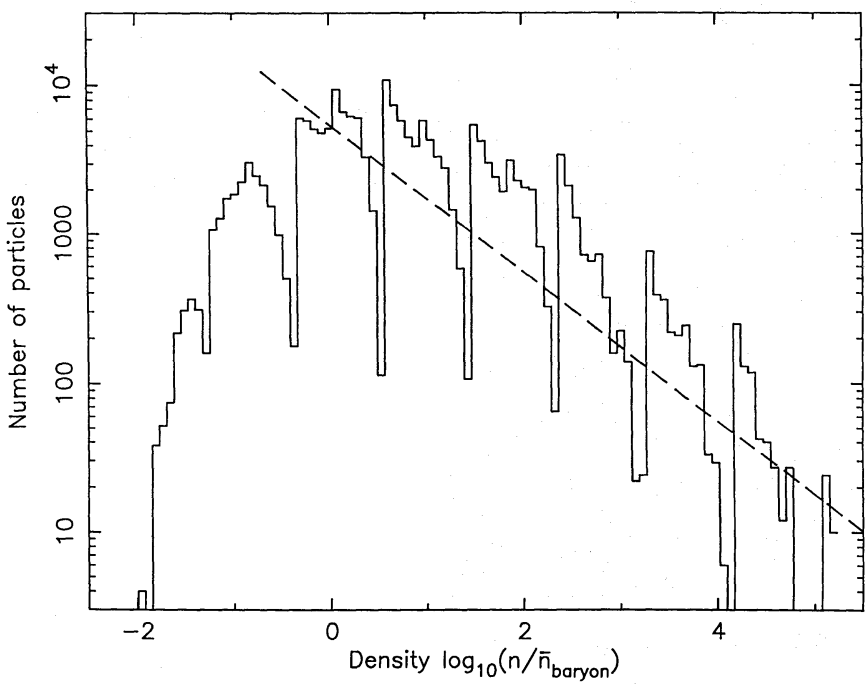

Figure 3. A histogram showing the density distribution of particles in the 40-Mpc simulation at $z=0$. The dashed line represents $N(>n)\propto n^{-1/2}$. The volume is divided until there are approximately four particles in a sampling box – hence the apparent periodicity.

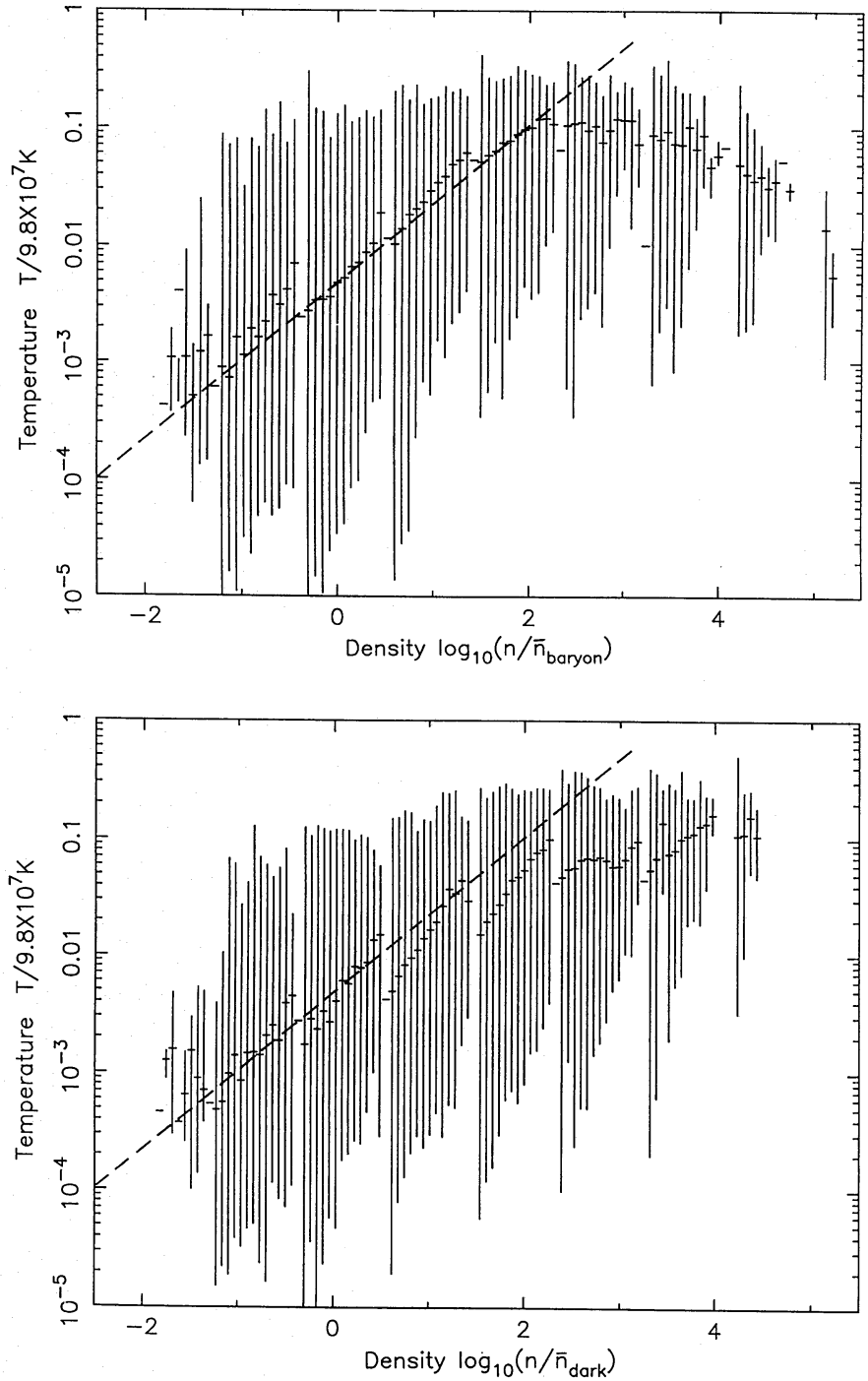

Figure 4. (a) The 'phase diagram' of the gas at $z=0$. The error bars show the full range of temperatures, measured using at least 4 particles. The dashed line represents $T \propto n^{2/3}$. (b) As Fig. 4(a) but for the dark matter.

temperatures in this diagram it is important to distinguish the properties of the 'gas particles' from those of the IGM which they represent. What we are plotting is the random kinetic energy of $1.5\times10^9 M_\odot$ clouds and it is only in virialized haloes that this will be equal to the gas temperature. At the initial time the gas-particle distribution is approximately isothermal at a temperature of 6.5×10^4 K, corresponding to the random motions induced by the $\sim 1.5\times10^{10} M_\odot$ dark particles at the mean separation. The gas, originally clustered around the mean density, will expand adiabatically so that over a large range of densities the equation of state is approximately adiabatic, $T\propto\rho^{2/3}$, as shown on the diagram. This agreement is somewhat fortuitous, however, as the measured 'temperature' does not decrease with time as rapidly as suggested by adiabatic expansion [i.e. $(1+z)^2$]. There are several reasons for this:

(i) Gravitational interactions between pairs of particles may lead to increased random velocities.

(ii) In low-density regions there are insufficient particles to resolve the voids and so we are measuring the expansion relative to the Hubble frame.

(iii) There is extensive heat conduction from collapsed haloes into the surrounding medium; this is clearly seen in the temperature profiles of clusters which remain almost isothermal out to large radii and low densities. Note that it is not necessary for particles to escape from the cluster in order for conduction to take place, as collisions may happen at a distance. Conduction is less important in the dark matter as there is no interaction between bound halo particles and those in the IGM. This can be seen in the phase diagram which shows lower temperatures than that of the gas for overdensities in the range 3–1000.

In the gas there is a slight tendency for very high-density material to be cooler. This is consistent with the notion that these regions formed at slightly higher redshifts and survived heirarchical disruption. No such effect is seen in the dark matter in which such substructure is erased by merging, and phase mixing (i.e. interpenetration of the particle flows) leads to an approximately isothermal structure.

4 Discussion

4.1 CLUSTERS AND X-RAYS EMISSION

Fig. 5 shows a projection through the gas distribution at the final time. The solid lines enclose regions which contain gas with an overdensity of 100 or more – roughly corresponding to the positions of virialized clusters, and the dotted lines overdensities of 10 or more. We require at least 4 particles (corresponding to $6\times10^9 M_\odot$) in order to define the density and so large regions of the diagram appear void, even though the galaxies in them may actually contain some gas.

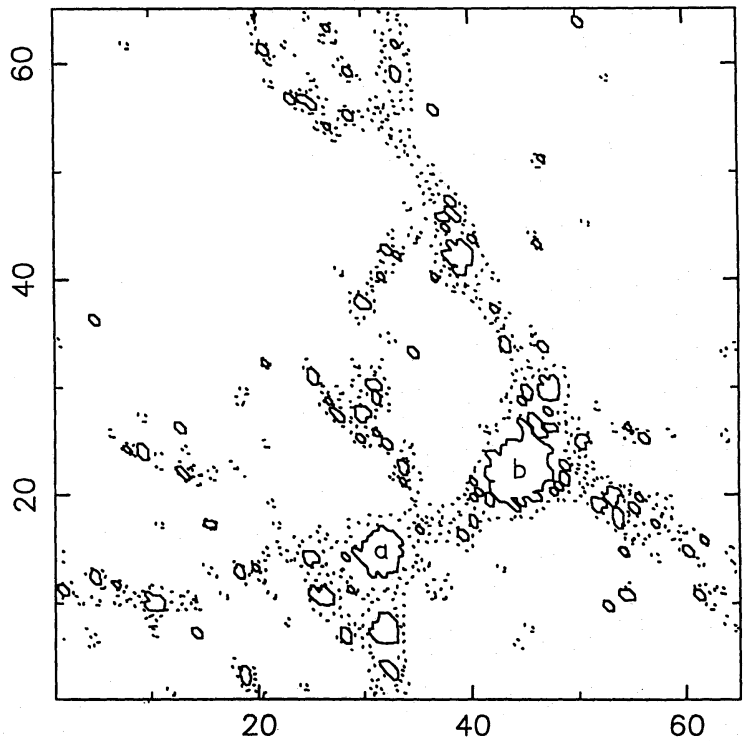

Figure 5. The maximum density of the gas along a projection through the simulation at the final time. The solid and dotted lines enclose overdensities of 100 and 10, respectively.

Fig. 6 shows the relative density profiles of gas, stars and dark matter across the two largest condensations seen in Fig. 5. The constant mass ratio of the components, 2:1:30, is similar to that in the simulation as a whole, confirming that star formation is unbiased on cluster scales. In both cases the temperature of each component is uniform at $1-2\times10^7$ K across most of the group. The galaxy distributions are more concentrated than that of the stars shown here. Despite the large size of the gas particles, which makes detailed modelling suspect, it is tempting to identify much of the loose stellar distribution with the diffuse background light and cD envelopes often seen around the central giant elliptical galaxy in clusters of galaxies (Oemler 1976; Thuan & Romanishin 1981).

The larger of the two clusters shown above, labelled (b), has an extended core with no dominant galaxy and has recently formed by the merger of several subgroups which contain denser and cooler gas. The other, (a), is more regular. It is dominated by a large central galaxy ($\sim 2\times10^{13}M_\odot$) extending out to 300 kpc. The central cooling time is less than a Hubble time and so, were the algorithm to allow cooling at this temperature, a cooling flow would result. The mass flux would be $80M_\odot$ yr^{-1} within 160 kpc, similar to that seen in nearby clusters (Arnaud 1985). The total X-ray emission from each of these clusters is $\sim 5\times10^{45}$ erg s^{-1} which is typical for those observed by the *Einstein Satellite* (Jones & Forman 1984). We should note that, although these large clusters dominate our impression of the simulation, most of the mass is contained in smaller objects.

The new generation of X-ray telescopes, ROSAT and AXAF, will be able to detect emission from haloes back to $z=1$ and beyond. This will provide strong constraint on the models and so it is worth asking how the X-ray emission has evolved in time. Kaiser (1986) has looked at the evolution of clusters (high-sigma objects) in hierarchical scaling models with power spectrum proportional to k^n. If the cooling function scales as T^α then the emission from a single halo $\propto mnT^\alpha$, where m is the mass and n the gas density. Thus it is always the high-mass objects that are most luminous at any given epoch. The largest objects, for which bremsstrahlung emission dominates, are less luminous at earlier times, whereas the smaller, more numerous haloes at temperatures below a few $\times10^6$ K (for which $\alpha\approx-1$) have higher luminosities at larger redshift. Halo luminosity decreases rapidly with increasing redshift once the cooling time of gas in a halo becomes less than the Hubble time, as it is this latter time-scale which limits the rate at which gas is supplied to the system.

The total luminosity density is given by the product of the individual halo luminosities with the space density of objects. At the current time high-mass objects dominate but at early epochs ($z\sim1$) there will be a greater contribution from the low-temperature gas in more numerous, low-mass haloes. The associated temperatures will be very low and will be difficult

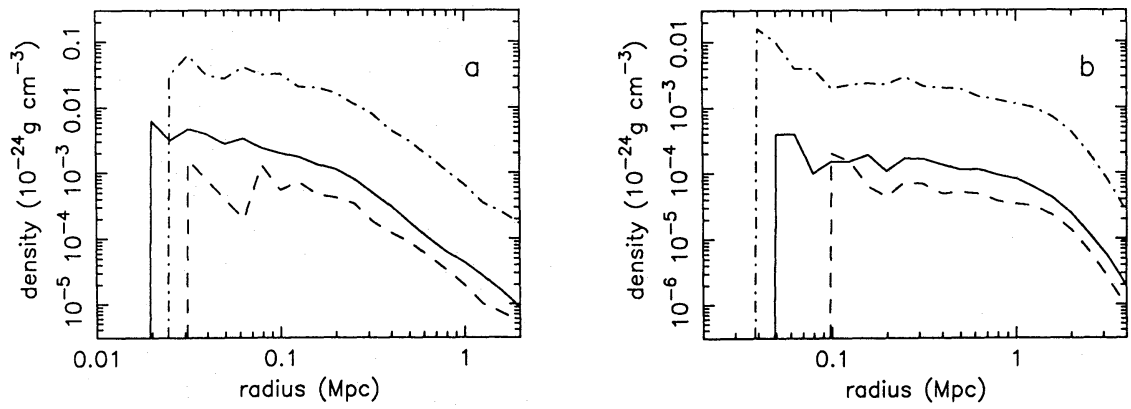

Figure 6. The density profiles of gas (——), dark matter (—·—·) and stars (– – –) within the two largest clusters (marked a and b on Fig. 5) in our simulation.

to detect, even in the soft X-ray bands, as galactic absorption will be important. Thus the behaviour of large clusters will be the most useful test of the theory.

This qualitative picture will be complicated by the details of the enrichment and cooling function of cluster gas, the rate at which gas is supplied by mergers etc., and more detailed models are needed before it can be used to discriminate between cosmological models. Some analytical calculations have been carried out by Cavaliere & Colafrancesco (1988); we intend to follow up our studies with models which incorporate smooth particle hydrodynamics for the gas.

4.3 SUNYAEV–ZEL'DOVICH EFFECT

Microwave photons scatter off hot electrons in collapsed objects, with a net increase in energy. This results in a reduced flux in the Rayleigh–Jeans part of the spectrum, corresponding to a lower temperature $T-\Delta T$. The apparent fractional decrease in temperature is proportional to the 'pressure column' along the line-of-sight (Sunyaev & Zel'dovich 1970):

$$y=\frac{\Delta T}{T}=\frac{1}{\Theta_b}\int\frac{2n_e kT_e\sigma_T}{m_e c^2}\,d\Theta_b\,dl, \tag{2}$$

where m_e, n_e and T_e are the electron mass, number density and temperature, k is the Boltzmann constant, σ_T the Thomson cross-section and c the speed of light, l is the line-of-sight distance and Θ_b the solid angle of the telescope beam. The value of $\Delta T/T$ varies with Θ_b depending on whether or not the dominant contributors are resolved by the beam. We will ignore this effect for now and look only at the general trends with mass and redshift.

The S–Z fluctuations in our simulations are measured by projecting the pressure column along one axis, into 64^2 cells. The resulting probability distributions for $\Delta T/T$ are given in Fig. 7 for various redshifts. Note that for $z\gtrsim 1$ the column may have been underestimated, as in our simulations gas is depleted from haloes very rapidly although this effect is less important for the large perturbations which have longer cooling times (see Section 3.2). The signal is dominated at late times by a few large clusters which have fluctuations over 100 times the mean (whereas the mode is 100 times smaller than the mean) i.e. the distribution is highly non-Gaussian.

We can understand this behaviour by considering simple scaling laws for the pressure column. The column through a single object of mass m is given by $(\Delta T/T)_m=n_e T_e r$, where $r\propto m^{1/3}(1+z_f)^{-1}$ is its radius and z_f the redshift of formation. In a simple hierarchical model with power spectrum $P_k\propto k^n$ then $m\sim(1+z_f)^{-6/(3+n)}$, and for virialized objects $T_e\propto m/r$. Putting all this together we can assess the relative contribution of different mass ranges at any given epoch:

$$\left\langle\frac{\Delta T}{T}\right\rangle\propto\int\left(\frac{\Delta T}{T}\right)_m r^2 N(m)\,dm\propto\int n_e m^{(11+n)/3}N(m)\,d(\log m), \tag{3}$$

where $N(m)\,dm$ is the number of clusters in the mass range $[m,m+dm]$. The electron density in a halo will lie somewhere between the density at time of formation $[\propto(1+z_f)^3\propto m^{-(3+n)/2}]$ and the density in recently-formed clusters. Thus the integrand in equation (3) is proportional to a power of m lying between $(11+n)/3$ and $(13-n)/6$. In either case, high-mass objects dominate as $N(m)$ diverges less rapidly than m^{-2} as $m\to 0$.

Fig. 7 shows that the mean value of the temperature fluctuations through our simulation [40/$(1+z)$ Mpc] remains approximately constant with time. This can also be explained in terms of

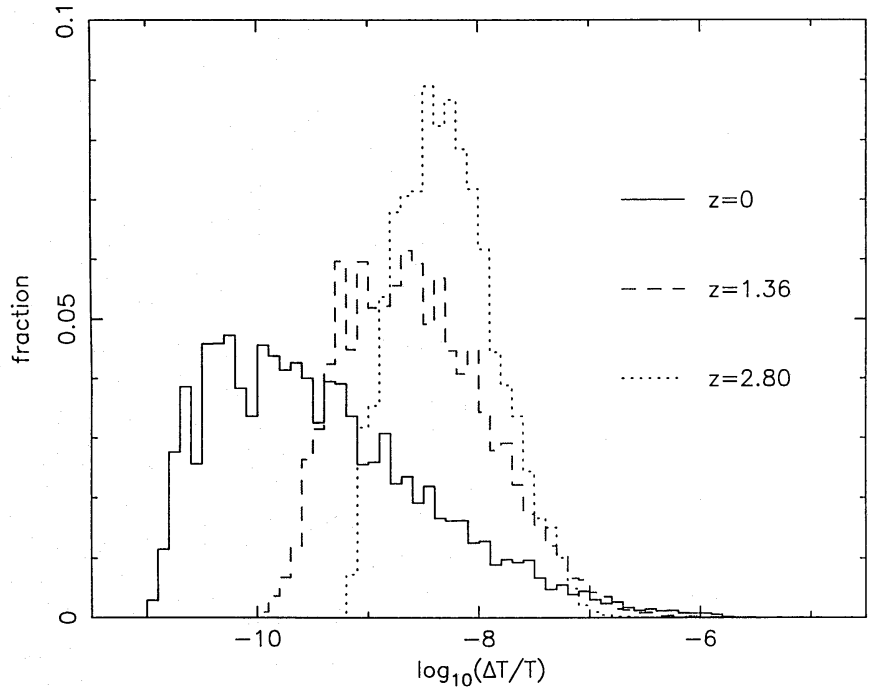

Figure 7. The probability distribution of $\Delta T/T$ projected along one axis of the simulation, at three different redshifts.

a simple hierarchical cosmology. Since we know that high-mass objects dominate, $\langle \Delta T/T \rangle$ is proportional to $\int N_x r_x^2 m_x n_e(m_x)\, dx$, where N_x is the comoving number density of high-mass, m_x, objects, $r_x \propto m_x^{1/3}$ is their comoving radius, $n_e \propto (1+z)^3$ their electron density and dx the comoving distance element. The integrand here is proportional to $(1+z)^{(5+3n)/(3+n)}$, which for cold dark matter gives little variation as n changes from -2 to -1 between the epochs of galaxy and cluster formation. The distribution becomes patchier at later times because the contribution from individual objects is greater. For resolved objects $(\Delta T/T)_m \propto m_x n_e \propto (1+z)^{3(1+n)/(3+n)}$ with a slow decrease back to $z \approx 1$, whereas for unresolved objects $(\Delta T/T)_m \propto m_x n_e (r/r_b)^2 \propto (1+z)^{[2(1+2n)/(3+n)]}/(\sqrt{1+z}-1)^2$ and the decrease is faster. In both cases $(\Delta T/T)_m$ decreases rapidly at higher redshifts when the cooling time is short and so the observed fluctuations are dominated by clusters at redshifts less than unity.

Fig. 8 shows the Sunyaev–Zel'dovich temperature fluctuations from a square degree patch when viewed with a resolution of 1 arcmin. The corresponding probability distribution is shown in Fig. 9. These results were obtained by stacking projections through our simulation at six different epochs, with random centres and orientations. Since these epochs do not represent independent pieces of space, further time resolution would not increase the data content. Each 40-Mpc box covers an interval of $40H_0/c = \frac{1}{150}$ in comoving coordinates. The distance to the horizon is two comoving units, and hence would require 300 separate projections. For the purpose of this measurement we only include 178 projections back to $z \approx 5$, before that the contributions are too small to be significant in a differential temperature measurement. With the simulations stacked, we simply choose a beam size and project it through the stack. For a beam of 1 arcmin^2 there are 400 separate samples even at a redshift of five, and many more at lower redshifts. Hence there is sufficient independent data to do our measurement. The gravitational softening length of 13 kpc subtends 1 arcmin at 40 Mpc; thus only for cluster cores nearer than 100 Mpc or so does our simulation fail to have adequate resolution.

The Sunyaev–Zel'dovich fluctuations shown in Fig. 8 represent only one realization of the Universe but we would expect others to differ only in minor details; using different random

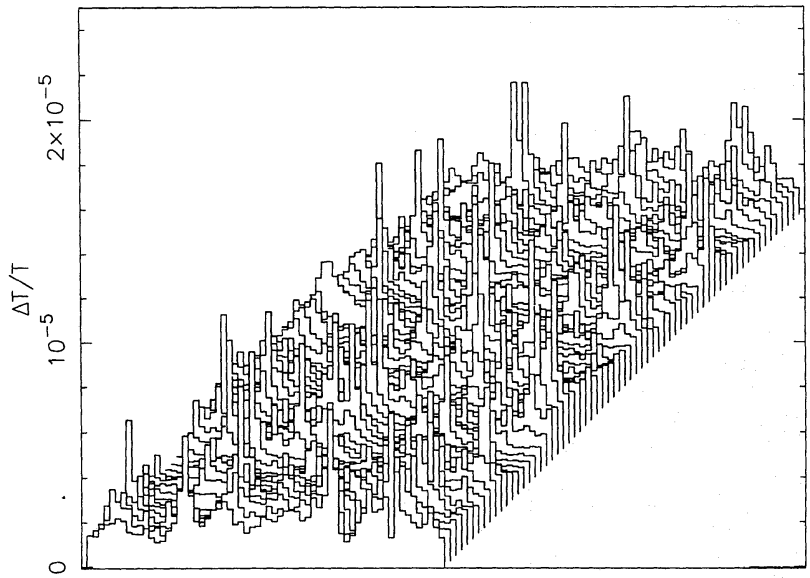

Figure 8. The Sunyaev–Zel'dovich fluctuations within a square degree projected back to $z \approx 5$ and viewed with a resolution of ~ 1 arcmin.

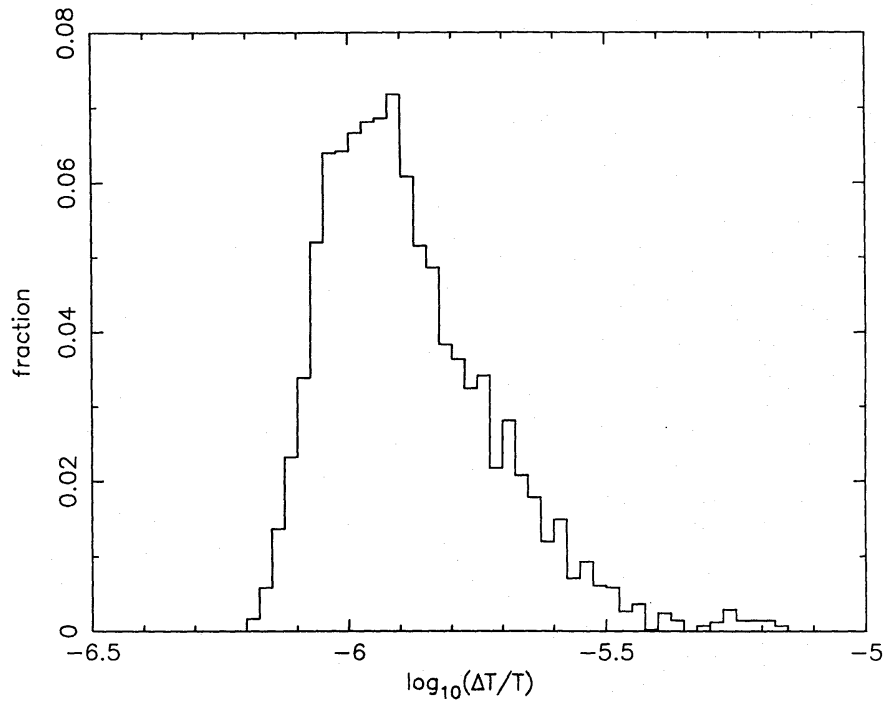

Figure 9. The probability distribution of $\Delta T/T$ for the fluctuations shown in Fig. 8.

numbers for the projections gives similar results. The standard deviation of the temperature decrement in 1-arcmin beams is 8×10^{-7}. Note that some papers give the root mean square (rms) fluctuations without removing the mean, which can be a much larger quantity – our measured rms fluctuation is 2×10^{-6}. For two beams which are close together on the sky the expected temperature difference is even smaller due to correlations between the temperature decrements. For example, we measure only one quarter the total variance for adjacent beams of 1 arcmin^2, increasing to the uncorrelated value at separations greater than about a quarter of a degree. The distribution of measured fluctuations is shown in Fig. 10. We point out that the standard deviation and angular correlation do not give a complete description of the

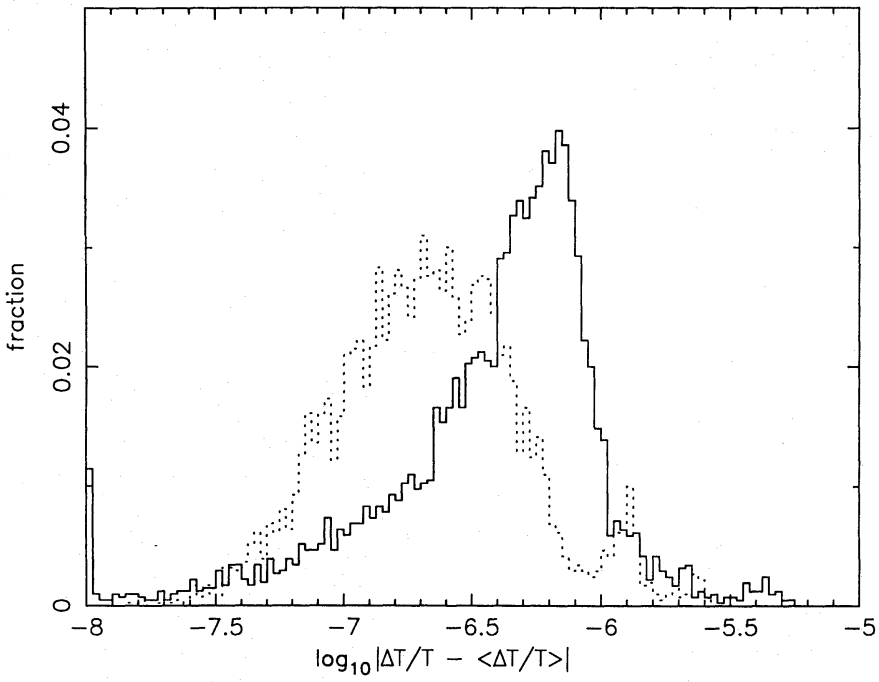

Figure 10. The solid line shows the probability distribution of deviations from the mean temperature decrement ($|\Delta T/T - \langle \Delta T/T \rangle|$), for the patch of sky simulated in Fig. 8. The dotted line shows the equivalent distribution which would be inferred by measuring temperature differences between adjacent 1-arcmin^2 beams.

fluctuations, as the actual distribution is not Gaussian; there are occasional large detections for lines-of-sight which happen to pass through large clusters.

Our result is similar in magnitude to that of Schaeffer & Silk (1988) but much smaller than most other estimates (e.g. Ostriker & Vishniac 1986, Bond 1988, Cole & Kaiser 1988). There are a number of effects which contribute to this difference:

(i) In the Press-Schechter (1974) formalism a factor of 2 is often introduced such that all the mass is then contained in virialized objects (not just that with an initial overdensity). In our simulation only about half the baryons lie in virialized clusters and one-third of these have formed stars, so our effective gas density is only one-third that of many analytic models, leading to a difference in normalization between our results and others. (For a discussion of the fits to the Press–Schechter model see CC88.)

(ii) One major problem with the analytic approaches is how to normalize the Sunyaev–Zel'dovich fluctuations through a typical cluster. For example, Bond (1988) argues for an early turn-around and large core radius of clusters in order to reproduce the observed number density of rich clusters. Cole & Kaiser normalize to a 1D velocity dispersion for Abell richness class 1 clusters of 750 km s^{-1}, whereas the X-ray temperatures give a lower normalization (the 'β-problem', Mushotzky 1984). Our simulation is normalized to give the correct correlation function of galaxies and should avoid these difficulties. Unfortunately we do not get a large cluster and so we cannot check to see that they would look like nearby Abell clusters. We suspect that we would find a relatively low temperature for rich clusters – it is possible that our final state is slightly underevolved.

(iii) The (40-Mpc)^3 box is not big enough to contain a cluster of Abell richness class 1 or greater. The analysis of Bond (1988) suggests that the dominant contributors to the variance are small clusters of size similar to those which we find in our box. Our standard deviation is too low but by a factor which is unlikely to exceed 1.5. More important is the fact that large clusters can add considerably to the high $\Delta T/T$ tail. X-ray observations (e.g. Jones & Forman 1984) suggest that values of $\sim 3 \times 10^{-5}$ could be attained through the cores of many clusters.

Several groups have reported detections of $\sim 10^{-4}$ in 0016+16, A665, A2218 and A401 and have inferred core values three times larger than this (Birkinshaw 1986; Uson 1986; Chase *et al.* 1987). The large column densities and temperatures required suggest that these would have to be very massive clusters.

(iv) Clustering of galaxies and clusters of galaxies will add to the variance but on a scale of 1 arcmin these effects will be small compared to the mean signal through any one cluster (Bond 1988).

(v) The fluctuations are proportional to the baryon density and the Hubble constant.

It is clear from this discussion that our simulation will underestimate the Sunyaev–Zel'dovich fluctuations – we feel that most analytic calculations overestimate them and that the true result will lie somewhere in between. Unfortunately our simulation cannot resolve density fluctuations on scales much smaller or much larger than 1 arcmin, however, we see no reason to doubt the models, which show a slight rise at smaller beam sizes and a more rapid decline at larger ones. Thus, even though the normalization is not precisely determined, we can safely conclude that for the Cold Dark Matter cosmology fluctuations in the microwave background which are larger than $\sim 10^{-5}$ will not be due to the Sunyaev–Zel'dovich effect unless there is a large cluster visible along the line-of-sight (back to $z \approx 1$). On scales smaller than about 1 arcmin the Sunyaev–Zel'dovich fluctuations may become larger than the primordal ones (Bond & Efstathiou 1984) but on larger scales they should be relatively unimportant.

5 Conclusions

We have discussed in some detail the behaviour of the baryonic component of cosmological *N*-body simulation. Our algorithm does not follow the cooling of the gas in detail but is sufficient to give the two desired effects:

(i) In regions where the cooling time is shorter than the dynamical, or Hubble, time gas cools to form stellar material.

(ii) The gas dissipates as it cools so that the resultant galaxy is sufficiently bound to survive hierarchical clustering.

There are ways in which our algorithm could be improved to simulate the gas physics more closely, however, they are unlikely to have a substantial effect on the results. The current cosmological *N*-body simulations do little more than identify the sites of galaxy formation. It is the gas physics, including feedback of energy and metals into the intracluster medium, which will determine the structure, morphology, mass–luminosity relation etc. Such detailed modelling is not yet available.

At the final time approximately one-third of the gas has turned into stars with little biasing on large (cluster-sized) scales. About half the residual is distributed in isothermal, $n \propto r^{-2}$, haloes with less than one-fifth remaining in underdense regions. The X-ray emission from present-day clusters resembles that observed by the *Einstein Satellite*; the evolution of cluster X-ray emission with redshift promises to be a strong constraint on cosmological models in the future.

We confirm the analytic calculations of previous authors who have argued that, within the CDM model, the Sunyaev–Zel'dovich fluctuations in the microwave background should be relatively small except through the cores of clusters of galaxies. Our simulations give qualitatively similar but slightly smaller effects (resulting from a difference in normalization to present day clusters). We may conclude, however, that microwave background fluctuations

greater than $\Delta T/T \sim 10^{-5}$ will not be due to the Sunyaev–Zel'dovich effect unless a cluster of galaxies is visible along the line of sight, back to $z \sim 1$.

Acknowledgments

PAT was supported during this research by the NSERC. The simulations were carried out using the facilities of the Pittsburgh Supercomputing Centre.

References

Arnaud, K. A., 1985. *PhD thesis,* Cambridge University.
Audouze, J., 1987. *Dark Matter in the Universe, IAU Symp. No. 117,* p. 499, eds Kormendy, J. & Knapp, G. R., Reidel, Dordrecht.
Birkinshaw, M., 1986. *Proc. NRAO Workshop no. 16,* p. 261, eds O'Dea, C. P. & Uson, J. M., NRAO.
Bond, J. R., 1988. In: *Proceedings of NATO Summer School on the Early Universe,* p. 287, ed. Unruh, W., Reidel, Dordrecht, Holland.
Bond, J. R. & Efstathiou, G., 1984. *Astrophys. J.,* **285,** L45.
Carlberg, R. G., 1988a. *Astrophys. J.,* **324,** 664.
Carlberg, R. G., 1988b. *Astrophys. J.,* **332,** 26.
Carlberg, R. G. & Couchman, H. M. P., 1988. *Astrophys. J.,* **340,** 47.
Cavaliere, A. & Colafrancesco, S., 1988. *Astrophys. J.,* **331,** 660.
Chase, S. T., Joseph, R. D., Robertson, N. A. & Ade, P. A. R., 1987. *Mon. Not. R. astr. Soc.,* **225,** 171.
Cole, S. M. & Kaiser, N., 1988. *Mon. Not. R. astr. Soc.,* **233,** 367.
Gunn, J. E. & Peterson, B. A., 1965. *Astrophys. J.,* **142,** 1633.
Jones, C. & Forman, W., 1984. *Astrophys. J.,* **276,** 38.
Kaiser, N., 1986. *Mon. Not. R. astr. Soc.,* **222,** 323.
Mushotzky, R. F., 1984. *Phys. Ser.,* **T7,** 151.
Ostriker, J. P. & Vishniac, E. T., 1986. *Astrophys. J.,* **306,** L51.
Oemler, A., Jr, 1976. *Astrophys. J.,* **209,** 693.
Press, W. H. & Schechter, P., 1974. *Astrophys. J.,* **187,** 425.
Rees, M. J. & Ostriker, J. P., 1977. *Astrophys. J.,* **179,** 541.
Rothenflug, R. & Arnaud, M., 1985. *Astr. Astrophys.,* **144,** 431.
Sarazin, C. L., 1986. *Rev. Mod. Phys.,* **58,** 1.
Schaeffer, R. & Silk, J., 1988. *Astrophys. J.,* **333,** 509.
Silk, J., 1977. *Astrophys. J.,* **211,** 638.
Sunyaev, R. A. & Zeldovich, Ya. B., 1970. *Astrophys. Space Sci.,* **7,** 3.
Thuan, T. X. & Romanishin, W., 1981. *Astrophys. J.,* **248,** 439.
Ulmer, M. P., Cruddace, R. G., Fenimore, E. E., Fritz, G. G. & Snyder, W. A., 1987. *Astrophys. J.,* **319,** 118.
Uson, J. M., 1986. *Proc. NRAO Workshop no. 16,* p. 261, eds O'Dea, C. P. & Uson, J. M., NRAO.
White, S. D. M. & Rees, M. J., 1978. *Mon. Not. R. astr. Soc.,* **183,** 341.
Yang, J., Turner, M. S., Steigman, G., Schramm, D. N. & Olive, K. A., 1984. *Astrophys. J.,* **281,** 493.
Zeldovich, Ya. B. & Sunyaev, R. A., 1969. *Astrophys. Space Sci.,* **4,** 301.